AIP Advances

Probing the charge recombination in rGO decorated mixed phase (anatase-rutile) TiO_2 multi-leg nanotubes

Cite as: AIP Advances **6**, 115010 (2016); https://doi.org/10.1063/1.4967387
Submitted: 03 October 2016 • Accepted: 24 October 2016 • Published Online: 23 November 2016

Y. Rambabu, Manu Jaiswal and Somnath C. Roy

Probing the charge recombination in rGO decorated mixed phase (anatase-rutile) TiO_2 multi-leg nanotubes

Y. Rambabu, Manu Jaiswal, and Somnath C. Roy[a]
Department of Physics, Indian Institute of Technology Madras, Chennai 600036, India

(Received 3 October 2016; accepted 24 October 2016; published online 3 November 2016)

Recombination of photo-generated charges is one of the most significant challenges in designing efficient photo-anode for photo electrochemical water oxidation. In the case of TiO_2, mixed phase (anatase-rutile) junctions often shown to be more effective in suppressing electron-hole recombination compared to a single (anatase or rutile) phase. Here, we report the study of bulk and surface recombination process in TiO_2 multi-leg nanotube (MLNTs) anatase-rutile (A-R) junctions decorated with reduced graphene oxide (rGO) layers, through an analysis of the photo-current and impedance characteristics. To quantify the charge transport/transfer process involved in these junctions, holes arriving at the interface of semiconductor/electrolyte were collected by adding H_2O_2 to the electrolyte. This enabled us to interpret the bulk and surface recombination process involved in anatase/rutile/rGO junctions for photo-electrochemical water oxidation. We correlated this quantification to the electrochemical impedance spectroscopy (EIS) measurements, and showed that in anatase/rutile junction the increase in PEC performance was due to suppression in electron-hole recombination rate at the surface states that effectively enhances the hole transfer rate to the electrolyte. On the other hand, in rGO wrapped A-R MLNTs junction it was due to both phenomenon *i.e* decrease in bulk recombination rate as well as increase in hole transfer rate to the electrolyte at the semiconductor/electrolyte interface. [http://dx.doi.org/10.1063/1.4967387]

I. INTRODUCTION

An efficient production of hydrogen through the photo electrochemical water splitting requires that the semiconducting material should efficiently absorb light to generate electron hole pairs and these charges can be separated quickly to minimize recombination.[1] A single material that can satisfy all the criteria has not been found so far and the practical solar-to-hydrogen conversion efficiencies are limited only to a few percent.

TiO_2 has so far been the most extensively studied photo-catalyst because of several qualities such as ease of processing, lack of toxicity, efficient electron-hole pair generation under the UV radiation, chemical stability and photo-corrosion resistance.[2,3] Various TiO_2 nanostructures such as, nanotubes, nanorods, nanofibers, nanoparticles *etc*. have been investigated as photo-electrodes for water splitting. However, the major bottle necks such as limited absorption of the visible light and higher recombination of the photo-generated charges are addressed through several strategies including doping,[4] decoration with metal and semiconductor nano-particles[5] and composite formation using other semiconductor materials.[6,7] In recent times, graphene and its derivatives (reduced graphene oxide-rGO) are also being investigated for improving the photo-catalytic/photovoltaic properties by forming composite with TiO_2.[8–10] It is reported that excellent electronic conductivity of this 2D material helps in the separation of photo-generated charges which, in turn,

[a]Corresponding Author. Email: somnath@iitm.ac.in

improves the catalytic activities. Furthermore, the layer morphology also helps in easy transport of the charge in the composite material.[11–13] Although, graphene composites with various nanostructures of TiO_2 had been investigated over the past couple of years, effective composite formation with the electrochemically anodized TiO_2 nanotubes remained a challenge due to compact morphology that prevented access to the outer surfaces of the nanotubes. We have recently shown that by using well-separated multi-leg single-phase TiO_2 nanotubes, a partial wrapping of rGO layers over the outer surfaces could be achieved, in which, rGO layers were also found to make interconnections between the adjacent nanotubes. An enhanced photocurrent has been observed in the rGO wrapped TiO_2 nanotubes that was attributed to the reduction of electron-hole recombination.[11]

On the other hand, it has also been shown that mixed phase (anatase-rutile) is more effective in improving PEC performance compared to single phase of TiO_2 having either anatase or rutile component.[14–16] This has been attributed to the ability of mixed phase junction (anatase/rutile) in suppressing charge carrier recombination rates by prolonging life time of electron-hole pair due to charge transfer from one phase to the other, thus increases the charge separation rate.[16,17] However, there is no general conclusion obtained in the direction of charge transfer from one phase to the other.[18] In a recent work, we have demonstrated that the MLNTs annealed at 800 °C have mixed phase with an anatase/rutile ratio ~20:80 and stable multi-leg morphology.[19]

Here, we report on the study of charge recombination in TiO_2 multi-leg nanotube (MLNTs) anatase-rutile (A-R) junctions decorated with reduced graphene oxide (rGO) layers with the help of hole scavenger (H_2O_2).[20] A comparative systematic investigations shown for charge recombination phenomenon associated with rGO functionalized mixed phase TiO_2 nanotubes (A/R-rGO MLNTs), rGO functionalized anatase phase TiO_2 nanotubes (A-rGO MLNTs), bare anatase phase TiO_2 nanotubes (A-MLNTs) and bare mixed phase TiO_2 nanotubes (A/R-MLNTs) for PEC water splitting. Such an analysis so far has not been reported for rGO decorated mixed phase junctions of TiO_2. To get a deeper understanding about the synergistic effect of anatase/rutile/rGO junction, we quantitatively analyzed the obtained photocurrent j_{photo} of A/R-rGO MLNTs junctions by splitting into the product $j_{abs} \times \eta_{ct} \times \eta_{tr}$,[20] where j_{abs} is the maximum photocurrent density in ideal case under no losses in the system, η_{tr} is the fraction of holes that reach the surface of semiconductor (without recombination in the bulk of the semiconductor) and η_{ct} is the fraction of holes injected into the electrolyte (without recombination on the surface). The data obtained from the analysis of the photocurrent values have been correlated with Electrochemical Impedance Spectra (EIS) to achieve a detailed understanding of the charge recombination and transport occurring inside the semiconductor as well as at the semiconductor-electrolyte interface. This comprehensive study of the charge transfer process occurring at rGO modified TiO_2 mixed phase junctions show that the enhancement in photo-current corresponding to A/R-MLNTs junction is due the decrease in electron-hole recombination rate at the surface states of semiconductor (η_{ct}). However, in A/R-rGO MLNTs, the improvement in photocurrent is attributed to the enhancement of charge separation and transport (reduction of recombination) both in the bulk semiconductor (η_{tr}), as well as across at the semiconductor/electrolyte interface (η_{ct}).

II. SYNTHESIS OF MULTI-LEG NANOTUBES

TiO_2 multi-leg nanotubes (MLNTs) were synthesized by electrochemical anodization method.[11,19] Prior to anodization Ti foil was cleaned with soap solution as well as ultrasonicated in a solution mixture consists of acetone, isopropyl alcohol and de-ionized water in equal volumes for 30 min. The Ti foil was dried under nitrogen stream before mounting onto anodization set-up. The anodization was carried out for 2 hr. in an electrolyte mixture comprising of 96 ml Di-Ethylene Glycol (DEG, Fisher Scientific) and 0.6 wt% ammonium bi-fluoride salt ($NH_4F.HF$) and 4ml de-ionized water (Millipore) at a constant voltage of 60V. After anodization, the samples were rinsed thoroughly with isopropyl alcohol and de-ionized water and kept at room temperature for 1 hr. to dry. Subsequently as-prepared samples were annealed at 500 °C for 3hrs with heating and cooling rates of 1°C per minute for anatase phase formation and 800 °C for 15 minutes for desired mixed phase formation.

A. Electrophoretic deposition of reduced graphene oxide layers on TiO_2 nanotubes

For synthesis of reduced graphene oxide modified anatase and mixed phase nanotubes electrophoretic deposition method was employed. A two electrode setup, with TiO_2 nanotubes (on Ti metal foil) as anode and a Pt foil cathode were used to carry out deposition of rGO layers. Reduced graphene oxide aqueous solution (0.05 mg/mL) was used as electrolyte.[11] A constant voltage of 50 V was applied between two electrodes separated at distance of 2 cm for a time interval of 20-90 sec. to obtain MLNTs wrapped or inter connected with rGO layers. The amount of rGO deposition can be controlled via deposition time. Figure S1 shows the deposition time *vs.* photocurrent density, the optimum time found to be ~ 40 sec, to get maximum photocurrent density with optimum wrapping or interconnections.

B. Characterization and PEC measurements:

For surface morphology characterization of as prepared samples, a field-emission scanning electron microscope (FEI Quanta 400) was used. High resolution transmission electron microscopy (HR-TEM) measurements were performed using JEOL JEM 3010 microscope. X-ray diffraction studies were performed using Panalytical X'pert-pro instrument. Photo-electro-chemical measurements were carried out using CHI 6005E (CH Instruments, USA) electrochemical analyzer in 1M NaOH aqueous solution as well as in 1M NaOH+0.5 M H_2O_2 aqueous solution at room temperature using three-electrode configuration. All electrolytes were prepared using Millipore de-ionized water (18.2M Ω). As prepared samples of exposed area 0.25 cm^2 was used as the anode, a Pt wire and Ag/AgCl (KCl saturated) were used as counter and reference electrodes. Measured potential *vs.* Ag/AgCl was converted into potential *vs.* RHE using the formula $E_{RHE} = E_{Ag/AgCl} + E^0_{Ag/AgCl} + 0.059 \times pH$, where $E^0_{Ag/AgCl}$ =0.1976V at 25 °C was the standard potential of reference electrode (Ag/AgCl).The measurements were performed under 1 Sun illumination (100mW/cm^2) using 300 watt Xenon lamp (Oriel) equipped with AM 1.5G filter. Diffuse Reflectance measurements were performed using JASCO V-660 UV-VIS-NIR spectrophotometer equipped with an integrating sphere and standard $BaSO_4$ sample used as a reference. The maximum achievable photocurrent density under no losses in system, j_{abs}, was obtained from optical absorbance (A) using calculation shown in the supplementary material (Figure S2). The electrochemical impedance measurements (EIS) were performed in a frequency range of 0.1 Hz to 100 KHz; impedance spectra were fitted using *Z*-view software.

III. RESULTS AND DISCUSSION

Figure 1 shows the FESEM image of rGO modified TiO_2 mixed phase A/R-MLNTs. The vertically oriented, well-separated nanotubes with a stable multi-leg morphology present a robust platform for the wrapping of rGO onto the TiO_2 nanotubes annealed at 800 °C. As evident, the rGO layers

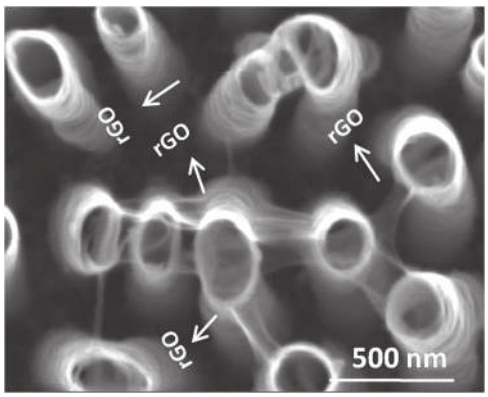

FIG. 1. FESEM shows the rGO layers wrapped/inter connected MLNTs with mixed phase A/R-rGO MLNTs.

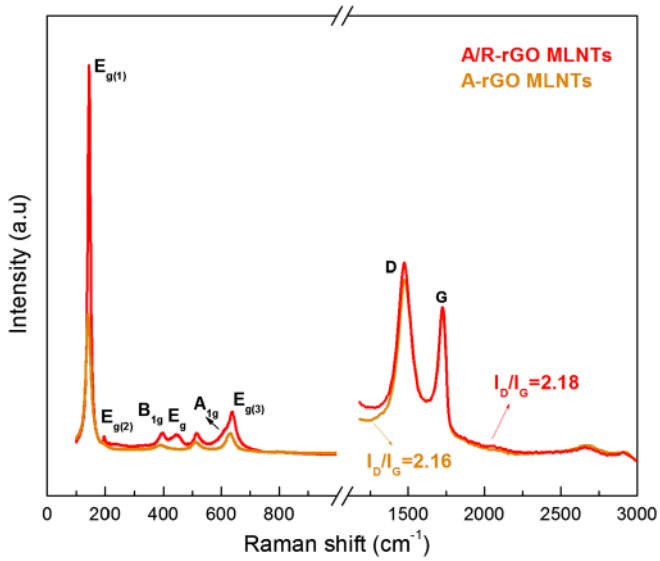

FIG. 2. Raman spectra of rGO wrapped/decorated anatase multi-leg nanotubes (A-rGO MLNTs) and mixed phase multi-leg nanotubes. The observation of D and G peaks confirm the presence of reduced graphene oxide layers on TiO_2 multi-leg nanotubes.

are not only wrapped around the nanotubes but also form inter connections between the adjacent nanotubes.

The weight ratio of anatase to rutile phases for rGO decorated TiO_2 MLNTs was estimated using the intensities of characteristic XRD peaks (Figure S3) corresponding to anatase and rutile phases and it was found to be ~20:80, consistent with our previous work.[19] Figure 2 shows the Raman spectra of rGO decorated anatase/rutile TiO_2 MLNTs. After deposition of rGO layers on TiO_2 MLNTs, the additional two peaks D-band and G-band were observed for A/R-rGO MLNTs, besides the TiO_2 peaks.[19,21,22] The D-band at 1328 cm^{-1} was attributed to disordered sp^2 bonded carbon atoms or defects and the G-band at 1596 cm^{-1} was attributed to ordered sp^2 bonded carbon network (graphitic structure, E_{2g} mode),[23,24] confirms deposition of rGO layers on TiO_2 MLNTs.

Figure 3 Shows the TEM and HR-TEM images of A-MLNTs obtained after annealing at 500 °C and A/R-MLNTs obtained after annealing at 800 °C. Figure 3(a) shows the HR-TEM image of lattice fringe spacing 0.35nm corresponding to (101) plane of anatase phase; inset shows the TEM image

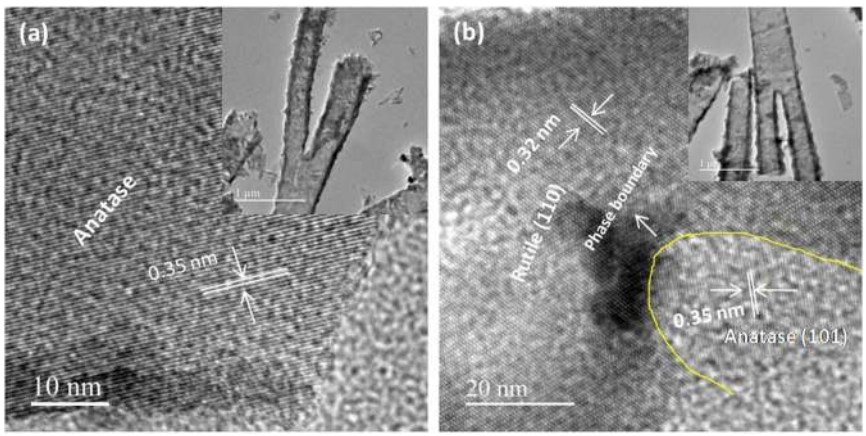

FIG. 3. HR-TEM images of as prepared photo anodes (a) lattice fringe spacing of anatase multi leg nano tubes annealed at 500 °C (A-MLNTs), inset shows nanotubes with two legs (b) lattice fringe spacing and phase boundary corresponding to anatase/rutile multi-leg nanotubes (A/R-MLNTs). (MLNT annealed at 800 °C), inset shows nanotubes with two legs.

of anatase multi-leg nanotubes in which we observe branching of single nanotube into two tubes. Figure 3(b) shows HR-TEM image of mixed phase TiO_2 nanotubes *i.e* A/R-MLNTs, marked line identifies the boundary of two phases, and also the image shows lattice fringe spacing corresponding to (101) plane of anatase and (110) plane of rutile phase. Inset shows the TEM image of structurally stable mixed phase branched nanotube. The TEM and HR-TEM results confirm that sample annealed at 500 °C possess single anatase phase, whereas for sample annealed at 800 °C possess mixed phase (anatase/rutile).

Figure 4 shows the photocurrent measurements carried out on different samples as photo anodes. The measured photocurrent densities at 1.23 V *vs.* RHE are: 0.23±0.01 mA/cm^2 for bare anatase multi-leg nanotubes (A-MLNTs), 0.34±0.01 mA/cm^2 for rGO modified anatase multi-leg nanotubes (A-rGO MLNTs), 0.29±0.01 mA/cm^2 for mixed phase bare A/R-MLNTs, and 0.63±0.01 mA/cm^2 for rGO modified mixed phase multi-leg nanotubes is (A/R-rGO MLNTs). The photocurrent data reveals that A-rGO MLNTs shows ~1.5 times, A/R-MLNTs (mixed phase) shows ~1.3 times, whereas A/R-rGO shows 2.7 times enhancement over that of A-MLNTs which represents synergistic effect of A/R-rGO junctions on the photocurrent performance.

To get an understanding of the factors influencing the photocurrent behavior and to analyze the charge transfer and recombination processes occurring in the photo anodes, we split the measured photocurrent into product $j_{photo} = j_{abs} \times \eta_{ct} \times \eta_{tr}$, where, j_{abs} is the maximum achievable photocurrent density under no losses in the system, η_{ct} is the fraction of holes transferred to the electrolyte without recombination with electrons at surface and η_{tr} is the fraction of photo generated charge carries (holes) that reach semiconductor/electrolyte interface without recombining with electrons in bulk semiconductor.[20,25–27] Hence the enhancement in photocurrent originate from (i) increase in absorbance, A of light *i.e* increase in j_{abs}, (ii) increase in charge separation rate or decrease in electron-hole recombination rate in bulk semiconductor *i.e* increase in η_{tr} and (iii) increase in rate of charge transfer process at the solid/liquid interface *i.e* increase in η_{ct}.[20,27]

To determine η_{tr} we measured the photocurrent in presence of a hole scavenger (0.5 M H_2O_2+ 1M NaOH aqueous solution), which is having oxidation potential much lower than that of H_2O and hence η_{ct} is considered to be unity.[20,27] A comparative photo current data (*j-V* plots) obtained for as prepared photo anodes with and without 0.5 M H_2O_2 in 1M NaOH electrolyte shown in Figure S4. By keeping $\eta_{ct}^{H2O2} = 1$, we get $j_{photo}^{H2O2} = j_{abs} \times \eta_{tr}$, from which we extracted η_{tr} and same is shown in Figure 5(a). The difference in the η_{tr} values among the samples indicates influence of phase content and rGO coverage on the charge transport/separation rate (recombination rate) inside the photo anode. The rGO modified mixed phase (anatase/rutile) nanotubes (A/R-rGO

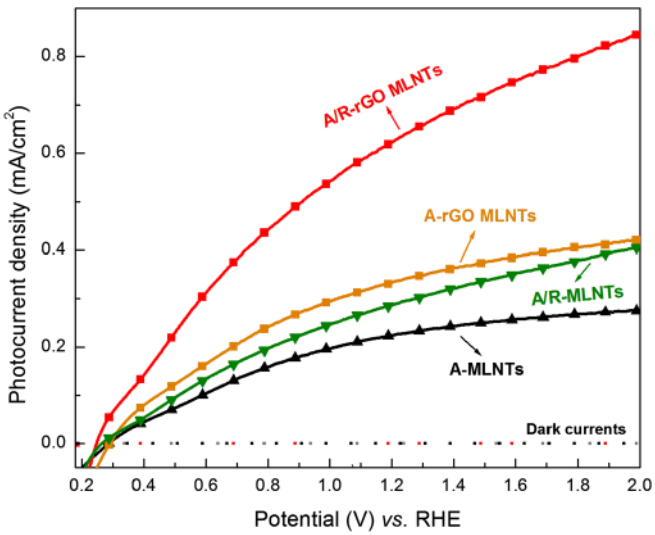

FIG. 4. *j-V* curves of as prepared photo anodes measured under 1 SUN illumination (100 mW/cm^2) in 1M NaOH aqueous solution.

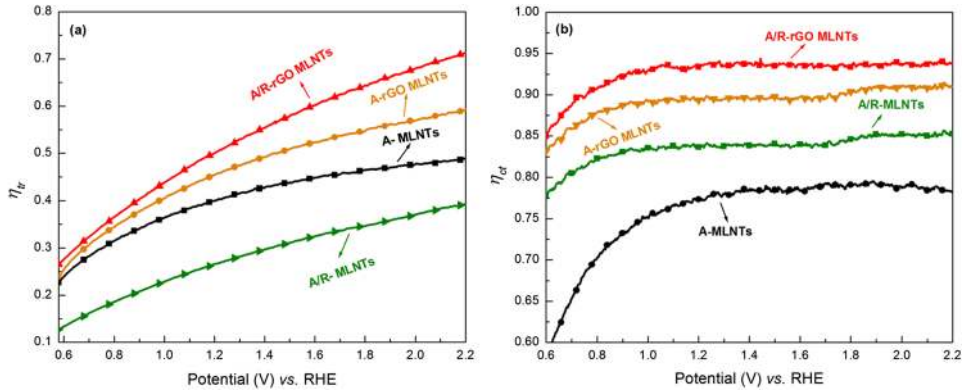

FIG. 5. Efficiencies of photo electrochemical sub processes in TiO_2 MLNT photo anodes. (a) Hole transport efficiency in bulk semiconductor η_{tr} as a function of V; A/R-rGO MLNTs and A-rGO shows higher η_{tr} and is in quantitative agreement with measured photo-current, however η_{tr} corresponding to A/R-MLNTs is lower compared to A-MLNTs, and is in consistent with the EIS measurements (b) Hole transfer efficiency η_{ct} at the semiconductor/electrolyte interface as a function of V; The A/R-rGO MLNTs photo anode shows higher η_{ct} followed by A-rGO MLNTs, A/R-MLNTs and bare A-MLNTs the trend is in quantitative agreement with the obtained photocurrent density.

MLNTs) and rGO modified anatase phase nanotubes (A-rGO MLNTs) show higher hole transport efficiency (η_{tr}) compared to that of bare A-MLNTs and A/R-MLNTs. This implies that the partially wrapped/interconnected TiO_2-rGO composite system promote the hole transport within the photo anode by significantly suppressing the charge recombination rate. The role of rGO in promoting charge transport is analyzed by conducting EIS measurements and discussed in next section. Further, we extracted η_{ct} by dividing photocurrent measured in absence of H_2O_2 (j_{photo}) with the photocurrent measured in presence of H_2O_2 in the electrolyte (j_{photo}^{H2O2}), i.e $\eta_{ct} = j_{photo}/j_{photo}^{H2O2}$. Figure 5(b) shows the obtained η_{ct}, and is higher for A/R-rGO MLNTs, followed by A-rGO MLNTs, A/R-MLNTs and A-MLNTs. This implies that the rGO modification and mixed phase junction formation significantly influencing hole transfer efficiency at the semiconductor/electrolyte interface. The discrepancies in hole transfer efficiency (η_{ct}) and hole transport efficiency (η_{tr}) of as prepared photo anodes indicates the difference in charge recombination process involved in the photocurrent performance of each photo anode.

To correlate the behavior of charge (hole) transport (η_{tr}) and charge (hole) transfer (η_{ct}) efficiencies to the PEC performance of the samples and to evaluate the bulk and surface recombination process involved in photo anodes, we conducted electrochemical impedance measurements (EIS) in a frequency range of 0.1Hz to 10^5 Hz. A representative Nyquist plots obtained for all photo-electrodes at 0.25 V *vs.* RHE shown in Figure 6(a). The obtained impedance data at each potential *vs.* RHE are fitted into two RC circuits connected in series to another series resistance; the circuit diagram shown in Figure 6(b). The equivalent circuit consists of a series resistance R_s representing solution resistance and/or bulk contact resistance, one RC circuit assigned to the charge transport in the bulk semiconductor nanostructure (A-MLNTs, A-rGO MLNTs, A/R-MLNTs and A/R-rGO MLNTs), and the other RC circuit represents charge transfer at the semiconductor/electrolyte interface junction. In the first RC circuit, R_{sc} is the internal bulk charge transport resistance or electron-hole recombination resistance and a constant phase element ($CPE1$) represents charge diffusion in the space charge layer or space charge layer capacitance (C_{SC}). In the second RC circuit, R_{ct} corresponds to the charge (hole) transfer resistance across the semiconductor/electrolyte interface and the constant phase element ($CPE2$) represents surface state capacitance or capacitance (C_{SE}) of double layer (sample/electrolyte interface).[11,28]

The constant phase element (CPE) can be expressed as

$$Z_{CPE} = \frac{1}{C} j\omega n^{-1} \tag{1}$$

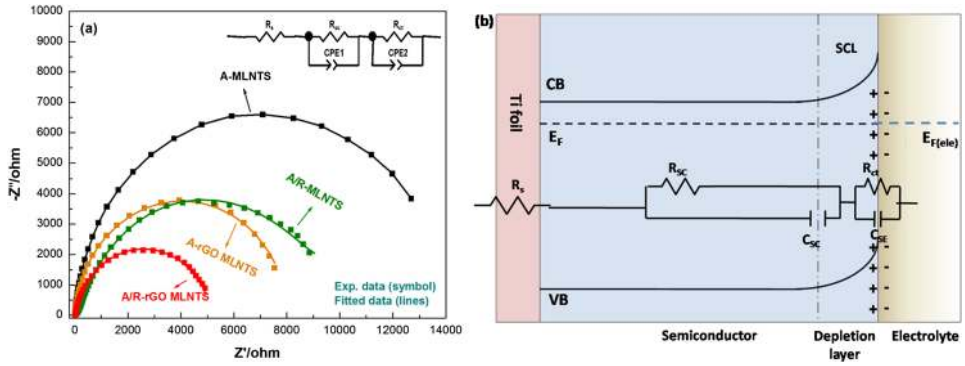

FIG. 6. (a) A representative Nyquist plots of as prepared bare A-TiO_2 MLNTs, A/R-TiO_2 MLNTS, A-rGO/TiO_2 MLNTs and A/R-rGO MLNTs obtained in 1M NaOH solution at 0.25 V *vs*. RHE. An equivalent circuit (inset and Figure 6(b)) is used to fit the plots. Symbols are experimental one, solid curves are fitted one using the equivalent circuit shown in Figure 6(b). In Figure 6 (b), R_s is contact/solution resistance, R_{sc} is bulk charge transport resistance of semiconductor film, R_{ct} is charge transfer resistance. CPE1 represents the space charge layer capacitance (C_{SC}), CPE2 represents surface state capacitance corresponding to semiconductor/electrolyte interface (C_{SE}).

Where, C is real capacitance, j is an imaginary number, ω is angular frequency and deviation of n from 1 (for ideal capacitance behavior n=1) indicates microscopic roughness or slow adsorption of chemical species on nano-structured electrode.[11]

As shown in Figure 7(a), the series resistance R_s is practically constant for all samples, while, charge transport resistance or bulk electron-hole recombination resistance R_{SC} (the resistance which arises due to bulk electron-hole recombination) shown in Figure 7(b) is lower for A/R-rGO MLNTs and A-rGO MLNTs implying that rGO decoration significantly enhancing the

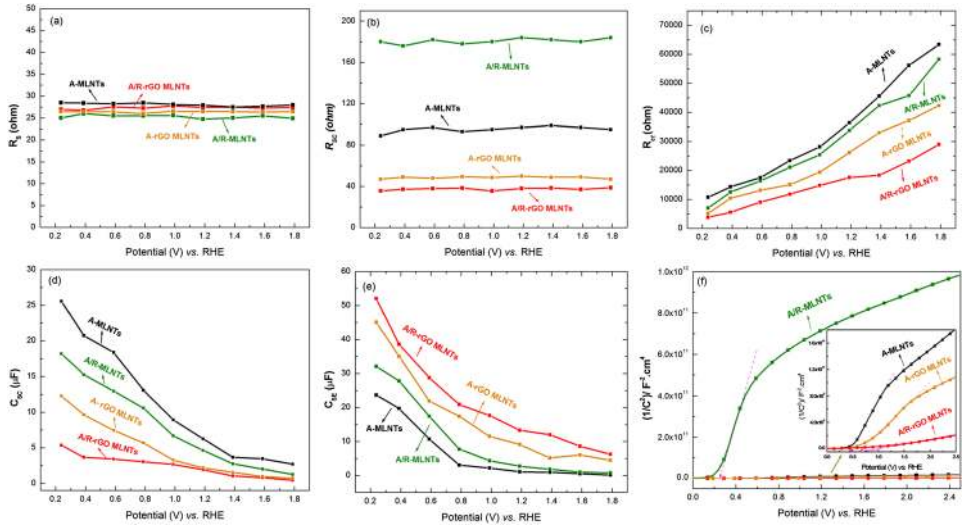

FIG. 7. Results obtained from electrochemical impedance spectroscopy (EIS) measurements. Figures a-e show the results of fitting Nyquist plots obtained under illumination with the equivalent circuit shown in supporting information (a) The bulk contact resistance R_S is practically constant for all photo anodes and is not depend on the applied potential (b) The bulk transport resistance R_{SC} is lower for photo anode A/R-rGO MLNTs and is higher for A/R-MLNTs, this in good agreement with η_{tr} (c) The photo anode/electrolyte charge transfer resistance R_{ct} is lower for A/R-rGO MLNTs followed by A-rGO MLNTs, A/R-MLNTs and A-MLNTs, well in agreement with the same quantitative trend shown by η_{ct} (d) Space-charge-layer capacitance measured under illumination, C_{sc} (e) The surface state capacitance, C_{SE} is higher for the A/R-MLNTs followed by A-rGO MLNTs, A/R MLNTs and A-MLNTs, in agreement with the trend shown in the photocurrent plots. (f) Mott-Schottky plots obtained from measurement of C_{SC} in the dark.

charge transport within the semiconductor. This is consistent with the observed hole transport efficiency η_{tr} in Figure 5(a). Further, it is to be noted that the obtained charge transport resistance R_{SC} (the resistance which arises due to bulk electron-hole recombination) is higher for A/R-MLNTs compared to that of bare A-MLNTs, indicates higher recombination rate and lower charge (hole) transport efficiency of A/R-MLNTs compared to A-MLNTs (consistent with the obtained η_{tr}). This is in agreement with the work by Kafizas *et al* which showed that the hole transfer from rutile to anatase can significantly increase anatase hole yield, (a 5 fold yield in 20:80 anatase: rutile junction) but does not substantially suppress the rate of electron-hole recombination within the semiconductor.[29]

However, the observed enhancement in photocurrent of A/R-MLNTs compared to A-MLNTs is attributed to the suppression in recombination of holes trapped by the surface states of the semiconductor, *i.e* decrease in recombination at the interface of semiconductor/electrolyte. This enhances the effective hole transfer to the electrolyte thus facilitates the rapid OER, and is consistent with the obtained lower hole transfer resistance R_{ct} (represents resistance corresponding to semiconductor/electrolyte interface) shown in Figure 7(c) and higher hole transfer efficiency to the electrolyte η_{ct} shown in Figure 5(b) compared to A-MLNTs. Hence, the hole transfer from rutile to anatase in A/R-MLNTs significantly reduces the electron-hole recombination at the interface of semiconductor/electrolyte or at the surface states, but not suppressing the bulk electron-hole recombination within the photo anode, which is confirmed by higher $R_{SC,}$ η_{ct} and lower $\eta_{tr,}$ R_{ct} of A/R-MLNTs than that of A-MLNTs. As mentioned earlier, this finding is well in agreement with the recent hole transfer study on mixed phase TiO_2.[29] Hence, the improvement in photocurrent of mixed phase TiO_2 compared to single anatase phase TiO_2 is due to increase in charge separation at the surface states but not due to the suppression in bulk electron-hole recombination within the semiconductor.

Further, it is to be noted that the charge transport resistance R_{SC} and charge transfer resistance R_{ct} of A/R-rGO MLNTs and A-rGO MLNTs is smaller compared to A/R-MLNTs and bare A-MLNTs, this is well in agreement with the same qualitative trend shown by η_{tr} and η_{ct} in Figure 5(a) and Figure 5(b). This implies decoration of rGO to A/R hetero junction drastically improves charge transport within the semiconductor as well as at the interface of semiconductor/electrolyte. This is attributed to the delocalized electrons present in the disordered sp^2 bonded graphitic network of carbon atoms and thus offers the lower resistant path to the photo excited electrons/holes of TiO_2 MLNTs, which means rGO acts like a sink to the photo generated charge carries generating from TiO_2 photo anode.[11]

Figure 7(d) shows the space charge layer capacitance and Figure 7(e) shows the surface state capacitance of the samples. The surface state capacitance (C_{SE}) is higher at onset potential for all photo anodes and it is gradually decreased upon increase in potential, which is due to the charging and discharging of surface states with holes. The observed higher surface state capacitance of A/R-rGO MLNTs and A-rGO MLNTs compared to that of A/R-MLNTs and bare A-MLNTs would facilitate the higher charge transfer to the electrolyte thus enhances the photo current, and is consistent with the observed η_{ct} in Figure 5(b).We calculated the total charge density Q_{SE} at the surface states by integrating C_{SE} with respect to V. The obtained Q_{SE} values are 32 μC, 24 μC, 14μC and 9μC for A/R-rGO MLNTs, A-rGO MLNTs, A/R-MLNTs and A-MLNTs, respectively, and it is in good agreement with the observed η_{ct}.

Figure 7(f) shows the Mott-Schottky measurements carried out for photo anodes at a frequency of 5000 Hz in the dark with scan rate 50 mV/s. Flat band potential was determined by the intersection of tangents drawn to the X-axis (potential axis). The flat band potential of A/R-rGO MLNTs (E_{FB}=0.99±0.03 V *vs.* RHE) and A-rGO MLNTs (E_{FB}=0.75±0.02 V *vs.* RHE) shifts towards positive side compared to A/R-MLNTs (E_{FB}=0.25±0.02 V *vs.* RHE) and A-MLNTs (E_{FB}=0.52±0.03 V *vs.* RHE). This indicates shift in Fermi level towards conduction band,[11,30] thus facilitating the efficient hole transfer to the electrolyte, and is consistent with the observed R_{ct}, $C_{SE,}Q_{SE}$ and η_{ct} values. The measured carrier density corresponding to A/R-rGO MLNTs (N_d=2.16±0.05×$10^{21}$$cm^{-3}$), A-rGO MLNTs ($N_d$=4.62±0.06×$10^{20}$ cm^{-3}) is higher compared to bare A-MLNTs (N_d = (2.12 ± 0.11) × 10^{20} cm^{-3}) also suggest the effective charge transport/transfer to the electrolyte thus enhances the PEC performance of A/R-rGO MLNTs.[30]

IV. CONCLUSIONS

In conclusion, we synthesized anatase/rutile/rGO junctions of TiO_2 nanotubes with stable multi-leg morphology. H_2O_2 used as an efficient hole scavenger to collect the holes that arriving at the semiconductor/electrolyte interface; this enabled to quantify the efficiencies of bulk charge recombination rate and surface state recombination process involved in A/R-rGO MLNTs, A-rGO MLNTs, A/R-MLNTs, and A-MLNTs. Using, electrochemical impedance spectroscopy is an effective technique and fitting the measured data to an equivalent circuit, we correlated the charge transport/transfer properties of as prepared photo anodes to the obtained efficiencies of bulk recombination process η_{tr} and surface charge recombination process η_{ct}. The improved PEC performance of A/R-MLNTs was due to increase in η_{ct} efficiency where as in A/R-rGO MLNTs it was due to increase in both the efficiencies η_{tr} and η_{ct}.

SUPPLEMENTARY MATERIAL

See supplementary material for figures showing (S1) variation of photocurrent density with rGO deposition time; (S2) optical absorption as function of wavelength obtained from the diffused reflectance spectra; (S3) X-ray diffractograms of the samples and (S4) photocurrent density vs. applied voltage for measured with and without hole scavenger (H_2O_2) added to the electrolyte.

ACKNOWLEDGMENTS

SCR thanks the Nissan Research Support Program at IIT Madras for financial support.

[1] Z. Chen, T. F. Jaramillo *et al.*, J. Mater. Res. **25**, 1 (2010).
[2] K. Hashimoto, H. Irie, and A. Fujishima, Japan. J. Appl. Phys. **44**, 8269 (2005).
[3] P. Roy, S. Berger, and P. Schmuki, Angew. Chem. Int. Edn. **39**, 502904 (2011).
[4] X. Tang and D. Li, J. Phys. Chem. C **112**, 5405 (2008).
[5] A. Mazare, N. Liu, K. Lee, M. S. Killian, and P. Schmuki, Chemistry Open **2**, 2 (2013).
[6] Q. Cai, H. Yang, Z. Hu, Z. Duan, Q. You, J. Sun, N. Xu, and J. Wu, Appl. Phys. Lett. **104**, 053114 (2014).
[7] S. Hernandez, D. Hidalgo, A. Sacco, A. Chiodoni, A. Lamberti, V. Cauda, E. Tresso, and G. Saracco, Phys.Chem.Chem.Phys. **17**, 7775 (2015).
[8] C. Chen, W. Cai, M. Long, B. Zhou, Y. Wu, D. Wu, Y. Feng, ACS Nano **4**, 6425(2010).
[9] Y. Tang, S. Luo, Y. Teng, C. Liu, X. Xu, X. Zhang, and L. Chen, Journal of Hazardous Materials **241**, 323 (2013).
[10] J. T. W. Wang, J. M. Ball, E. M. Barea, A. Abate, J. A. A. Webber, J. Huang, M. Saliba, I. M. Sero, J. Bisquert, H. J. Snaith, R. Nicholas, Nano Lett.**14**, 724 (2013).
[11] Y. Rambabu, M. Jaiswal, and S. C. Roy, Journal of The Electrochemical Society **163**, H652 (2016).
[12] G. Xie, K. Zhang, B. Guo, Q. Liu, L. Fang, and J. R. Gong, Adv. Mater. **25**, 3820 (2013).
[13] Y. Hau, I. V. Lightcap, K. Goodwin, M. Matsumura, P. V. Kamat, and J. Phys. Chem. Lett. **1**, 2222 (2010).
[14] J. Zhang, Q. Xu, Z. Feng, and M. Li, Angew. Chem. Int. Ed. **47**, 1766 (2008).
[15] Z. Y. Liu, X. Zhang, S. Nishimoto, M. Jin, D. A. Tryk, T. Murakami, A. .Fujishima, Langmuir **23**, 10916 (2007).
[16] D. C. Hurum, A. G. Agrios, K. A. Gray, T. Rajh, and M. C. Thurnauer, J. Phys. Chem. B **107**, 4545 (2003).
[17] X. Sun, W. Dai, G. Wu, L. Li, N. Guan, and M. Hunger, Chem. Commun **51**, 13779 (2015).
[18] A. Kafizas, C. J. Carmalt, and I. P. Parkin, Chem. Eur. J. **18**, 13048 (2012).
[19] Y. Rambabu, M. Jaiswal, S. C. Roy, Catalysis Today, 2016.
[20] H. Dotan, K. Sivula, M. Gratzel, A. Rothschild, and S. C. Warren, Energy Environ. Sci. **4**, 958 (2011).
[21] T. Oshsaka, F. Izumi, and Y. Fujiki, J. Raman Spectrosc. **7**, 321 (1978).
[22] W. F. Zhang, Y. L. He, M. S. Zhang, Z. Yin, and Q. Chen, J. Phys. D: Appl. Phys. **33**, 912 (2000).
[23] K. N. Kudin, B. Ozbas, H. C. Schniepp, R. K. Prudhomme, I. A. Aksay, and R. Car, Nano Lett. **8**, 36 (2008).
[24] D. Naumenko, V. Snitka, B. Snopok, S. Arpiainen, and H. Lipsanen, Nanotechnology **23**, 465703 (2012).
[25] P. M. Rao, L. Cai, C. Liu, I. S. Cho, C. H. Lee, J. M. Weiss, P. Yang, and X. Zheng, Nano Lett. **14**, 1099 (2014).
[26] T. W. Kim, Y. Ping, A. Galli, A. .Giulia, K. S. Choi, Nat. Commun. **6**, 8769 (2015).
[27] B. Iandolo, B. Wickman, E. Svensson, D. Paulsson, and A. Hellman, Nano Lett. **16**, 2381 (2016).
[28] Y. J. Kim, G. Magesh, D. H. Youn, J. Jang, J. Kubota, K. Domen, and J. S. Lee, Sci. Rep. **3**, 2681 (2013).
[29] A. Kafizas, X. Wang, S. R. Pendlebury, P. Barnes *et al.*, J. Phys. Chem. A **120**, 715 (2016).
[30] N. Zhang, Y. Zhang, X. Pan, M. Q. Yang, and Y. J. Xu, J. Phys. Chem. C **116**, 18023 (2012).